J. Plasma Phys. (2026), *vol*. 92, E112 © The Author(s), 2026. Published by Cambridge University Press.
This is an Open Access article, distributed under the terms of the Creative Commons Attribution licence (https://creativecommons.org/licenses/by/4.0/), which permits unrestricted re-use, distribution and reproduction, provided the original article is properly cited. doi:10.1017/S0022377826102025

Intermittent bursts induced by neoclassical double tearing modes reconnection via multihelicity simulation

Jincheng Wang[1], Tong Liu[1], Lai Wei[1] and Zheng-Xiong Wang[1]

[1]Key Laboratory of Materials Modification by Laser, Ion, and Electron Beams of the Ministry of Education, School of Physics, Dalian University of Technology, Dalian 116024, PR China

Corresponding author: Tong Liu, liutong@dlut.edu.cn

(Received 24 March 2026 UTC; revision received 6 June 2026 UTC; accepted 8 June 2026 UTC)

In the long-pulse steady-state operation of future advanced tokamaks, intermittent bursts induced by magnetohydrodynamic (MHD) instabilities present a critical challenge to plasma confinement. Therefore, the nonlinear dynamics of intermittent bursts induced by neoclassical double tearing modes in reversed magnetic shear plasmas are systematically investigated using a reduced MHD model in a cylindrical coordinate system. Comparisons between single-helicity (SH) and multihelicity (MH) simulation results reveal that the burst amplitude and average energy of the dominant $m/n = 3/1$ mode in the MH case are lower than those in the SH case. This phenomenon is mainly attributed to the redistribution of perturbation energy during the MH nonlinear coupling process: a portion of the magnetic free energy is transferred to the subdominant $m/n = 5/2$ mode and higher harmonics. Furthermore, an increased bootstrap current fraction modulates the intermittent bursting characteristics by reducing the ohmic current proportion, thereby weakening the q-profile restoration capability. Consequently, when the bootstrap current fraction (f_b) reaches a certain threshold ($f_b \geq 0.2$), the burst amplitude of the dominant mode tends to saturate, and the burst period begins to decrease gradually. Particularly at a high bootstrap current fraction ($f_b \geq 0.4$), constrained by the suppressed overall energy level, the MH system maintains only a weak relaxation process, exhibiting greater reductions in burst amplitude and period than the SH case.

Key words: fusion plasma, plasma instabilities, plasma simulation

1. Introduction

The reversed magnetic shear (RMS) configuration is assumed to be the ideal candidate for the steady-state operation of future advanced tokamaks (Gormezano *et al.* 2007; Kikuchi & Azumi 2012) because it can facilitate the formation of an internal transport barrier and significantly improve plasma confinement (Levinton *et al.* 1995; Strait *et al.* 1995; Kuiroukidis & Throumoulopoulos 2015). However, while providing high confinement performance, this configuration also introduces potential magnetohydrodynamic (MHD) instability risks (Ishii, Azumi & Kishimoto 2002;

Downloaded from https://www.cambridge.org/core. UNIVERSIDAD AUTONOMA METROPOLITANA, on 19 Nov 2026 at 14:11:34, subject to the Cambridge Core terms of use, available at https://www.cambridge.org/core/terms. https://doi.org/10.1017/S0022377826102025

Wang & Wang 2015). The RMS configuration features a non-monotonic safety factor q profile, which usually allows the coexistence of two rational surfaces with the same helicity ($h = m/n$) in the plasma (Furth, Rutherford & Selberg 1973; Feng *et al.* 2020; Zhang *et al.* 2020). Such a specific magnetic topology is highly susceptible to the double tearing mode (DTM) instability (Pritchett, Lee & Drake 1980; Fitzpatrick 1995). The nonlinear explosive growth of the DTM leads to the overlap of the inner and outer magnetic islands and the fast reconnection of magnetic field lines (Bierwage *et al.* 2005; Wang *et al.* 2007), causing severe degradation of plasma confinement performance and MHD stability (Dong, Mahajan & Horton 2003; Janvier, Kishimoto & Li 2011).

In addition to such disruptive events, periodic relaxation processes are also widely observed in long-pulse discharges. For instance, in positive magnetic shear tokamak plasmas, sawtooth oscillations in the central region are common periodic MHD activities (von Goeler, Stodiek & Sauthoff 1974; Chang *et al.* 1996). By contrast, in the RMS configuration, investigations into the long-pulse nonlinear evolution of the DTM indicate that the initial fast reconnection is often not the end of the evolution (Zhang *et al.* 2019). The system will evolve into a relaxation process in the off-axis region similar to the central sawtooth oscillations, manifesting as significant 'intermittent bursts' (Wei & Wang 2014*a*). Physically, this intermittent phenomenon is governed by a competitive process within the system: the competition between the energy release induced by magnetic island reconnection and the restoration of the magnetic configuration dominated by the ohmic current in the total current. After the initial reconnection releases a large amount of free energy, the ohmic current drives the q profile to gradually restore towards the initial unstable state, thereby triggering continuous annular sawtooth crashes. Such continuous periodic bursting activities will constantly change the local magnetic topology, which may have a severe adverse impact on maintaining long-pulse steady-state operation in future advanced tokamaks.

Furthermore, the fraction of the bootstrap current in the total current increases significantly in the high poloidal beta (β_p) operation mode of advanced tokamaks (Zarnstorff *et al.* 1988; Ishida *et al.* 1992; Wang *et al.* 2011). This non-inductive current driven by the pressure gradient can reduce the dependence on external current drive, which is important for achieving the long-pulse steady-state operation of the device (Fujita *et al.* 2001). However, the presence of the bootstrap current can excite the neoclassical DTM (NDTM) (Buttery *et al.* 2000; Wang, Tang & Wei 2022*b*), thereby affecting the plasma confinement performance (Yu *et al.* 2000; Hu *et al.* 2023; Bardoczi *et al.* 2024). The study by Wang *et al.* showed that the bootstrap current modifies the nonlinear saturation level of the DTM (Wang, Wei & Yu 2015*b*). Based on this, further investigation into the long-pulse evolution process reveals that the bootstrap current has a significant impact on the intermittent bursting behaviour. Under the condition of maintaining the total current constant, as the bootstrap current fraction increases, the proportion of the ohmic current in the total current used to restore the magnetic configuration decreases correspondingly. This leads to a slower restoration process of the magnetic shear, a decrease in the average energy and amplitude of the intermittent bursts, and an extension of the burst period. Although a high bootstrap current fraction ($f_b \geq 0.4$) can suppress the subsequent periodic bursts, the initial reconnection crash still exists and continues to cause damage to the plasma.

It should be noted that in previous numerical studies, the nonlinear evolution of the intermittent bursts of the DTM was mostly limited to the single-helicity (SH)

Downloaded from https://www.cambridge.org/core. UNIVERSIDAD AUTONOMA METROPOLITANA, on 19 Nov 2026 at 14:11:34, subject to the Cambridge Core terms of use, available at https://www.cambridge.org/core/terms. https://doi.org/10.1017/S0022377826102025

approximation (Wei *et al.* 2012), i.e. only the fundamental mode and its higher harmonics were considered (Matsumoto *et al.* 2005). However, realistic tokamak plasmas are three-dimensional complex systems containing multiple modes with different helicities (Jardin, Ferraro & Krebs 2015). Multihelicity (MH) simulations have shown that the coupling between modes with different helicities alters the nonlinear evolution process of the system (Wei & Wang 2014*b*; Bardoczi, Logan & Strait 2021). Therefore, the inclusion of MH coupling represents an essential extension beyond the SH approximation, because it allows the perturbation energy to be redistributed between different helicities and modifies the nonlinear evolution of the dominant mode. During the intermittent bursting process, the MH coupling leads to a redistribution of energy: a portion of the magnetic free energy is transferred to the subdominant modes and the higher harmonics generated by their coupling, making the burst intensity of the dominant mode lower than that in the SH case. Meanwhile, the spatial overlap of multiple modes induces magnetic stochasticity (Bierwage *et al.* 2005; Yu 2007). When the bootstrap current effect is considered, this magnetic stochasticity leads to a local pressure flattening, which in turn causes the loss of the bootstrap current in that region. The change in the local current gradient provides an extra driving force, accelerating the dominant mode into the Rutherford growth regime (Wang, Wang & Wang 2013; Wang *et al.* 2015*a*; Wang, Liu & Wei 2022*a*).

The paper utilises a reduced MHD model with multiple helicities in a cylindrical geometry to numerically investigate the intermittent bursting characteristics of the NDTM in the RMS configuration. The simulation results reveal that the burst amplitude and average energy of the dominant mode are significantly reduced compared with the SH case, which is primarily attributed to the redistribution of perturbation energy during the MH nonlinear coupling process. Furthermore, a higher bootstrap current fraction fundamentally weakens the restoration capability of the safety factor q profile, driving the system into a weak relaxation regime that further reduces both the burst amplitude and period.

The remainder of this paper is organised as follows: § 2 presents the reduced MHD model including the bootstrap current term and the initial configuration set-up. Section 3 shows the nonlinear simulation results of the intermittent bursts of the NDTM, focusing on comparing and discussing the effects of the MH coupling and the bootstrap current fraction. Section 4 is a summary of the whole paper.

2. Modelling equations

In order to investigate the nonlinear dynamic evolution of NDTMs, a standard reduced MHD model in a cylindrical coordinate system (r, θ, z) is employed in this work (Strauss 1976; Hazeltine, Kotschenreuther & Morrison 1985; Sato & Wakatani 2005). The normalised governing equations are expressed as follows:

$$\frac{\partial \psi}{\partial t} = [\psi, \phi] - \partial_z \phi - S_A^{-1}(j - j_b) + E_{z0}, \tag{2.1}$$

$$\frac{\partial u}{\partial t} = [u, \phi] + [j, \psi] + \partial_z j + R^{-1}\nabla_\perp^2 u, \tag{2.2}$$

$$\frac{\partial p}{\partial t} = [p, \phi] + \chi_\parallel \nabla_\parallel^2 p + \chi_\perp \nabla_\perp^2 p + S_0. \tag{2.3}$$

Here, ψ, ϕ and p represent the poloidal magnetic flux, the stream function and the plasma pressure, respectively. The variables $j = -\nabla_\perp^2 \psi$ and $u = \nabla_\perp^2 \phi$ in

Downloaded from https://www.cambridge.org/core. UNIVERSIDAD AUTONOMA METROPOLITANA, on 19 Nov 2026 at 14:11:34, subject to the Cambridge Core terms of use, available at https://www.cambridge.org/core/terms. https://doi.org/10.1017/S0022377826102025

the equations denote the plasma current density and the vorticity along the axial direction, respectively. Under the reduced MHD approximation, assuming that the poloidal rotation is mainly provided by the $E \times B$ drift, the plasma velocity field can be expressed as $\boldsymbol{v} = -\nabla\phi \times \hat{z}$ (where ϕ is equivalent to the electrostatic potential) (Zhang & Ma 2009; Wang & Wang 2015). The nonlinear Poisson bracket included in (2.1)–(2.3) is defined as $[f, g] = \hat{z} \cdot (\nabla f \times \nabla g)$. The gradient operator parallel to the magnetic field is defined as $\nabla_{\parallel} S = \partial S/\partial z + [S, \psi]$.

A standard normalisation scheme is adopted in this model. For the spatial coordinates, the radial distance r is normalised by the plasma minor radius a. The time t and the velocity field v are normalised in units of the Alfvén time $\tau_A = a\sqrt{\mu_0\rho}/B_0$ and the Alfvén velocity $v_A = B_0/\sqrt{\mu_0\rho}$, respectively. Accordingly, the poloidal magnetic flux ψ, the stream function ϕ and the plasma pressure p are normalised by aB_0, aB_0v_A and the initial pressure at the magnetic axis, respectively. The expression $\beta_e = 2\mu_0 n_0 T_e/B_0^2$ is used to characterise the ratio of the thermal pressure to the magnetic pressure. The dimensionless dissipation coefficients are characterised by the magnetic Reynolds number $S_A = \tau_\eta/\tau_A$, the kinematic Reynolds number $R = \tau_v/\tau_A$ and the heat transport coefficients $\chi_{\parallel}$ and $\chi_{\perp}$. Here, $\tau_\eta = a^2\mu_0/\hat{\eta}$ and $\tau_v = a^2/\hat{\mu}$ denote the resistive and viscous diffusion times, respectively. The heat transport coefficients $\chi_{\parallel}$ and $\chi_{\perp}$ are both normalised to a^2/τ_A. The term j_b in (2.1) is the bootstrap current density driven by the radial pressure gradient, and its magnitude is determined by the bootstrap current fraction defined as $f_b = \int j_{b0} r\,\mathrm{d}r / \int j_{z0} r\,\mathrm{d}r$. Furthermore, the source terms $E_{z0} = S_A^{-1}(j_0 - j_{b0})$ and $S_0 = -\chi_{\perp}\nabla_{\perp}^2 p_0$ in (2.1) and (2.3) are chosen to balance the diffusions of the initial equilibrium profiles of the ohmic current ($j_{\mathrm{ohm}} = j_0 - j_{b0}$) and pressure, respectively.

Any physical variable $f(r, \theta, z, t)$ in the system can be decomposed into an initial equilibrium term $f_0(r)$ that is independent of time and a perturbation term $\tilde{f}(r, \theta, z, t)$ that evolves with time. By applying periodic boundary conditions in the poloidal and axial directions, the perturbed fields can be expanded via Fourier transform as

$$\tilde{f}\,(r, \theta, z, t) = \frac{1}{2}\sum\nolimits_{m,n} \tilde{f}_{m,n}\,(r, t)\exp\,(im\theta - inz/R_0) + c.c. \tag{2.4}$$

where m and n are the poloidal and toroidal mode numbers, respectively, and R_0 is the major radius of the tokamak. To analyse the magnetic reconnection process, the equilibrium helical flux associated with a given m/n perturbation is defined as

$$\psi^*_{m/n}(r) = \int_0^r r'\left[\frac{1}{q(r')} - \frac{n}{m}\right]\mathrm{d}r'. \tag{2.5}$$

In cylindrical geometry, $\psi^*_{m/n}$ represents the equilibrium magnetic flux in the frame moving with the helical pitch of the m/n perturbation. Its radial derivative satisfies

$$\frac{\mathrm{d}\psi^*_{m/n}}{\mathrm{d}r} = r\left[\frac{1}{q(r)} - \frac{n}{m}\right], \tag{2.6}$$

so the stationary points of $\psi^*_{m/n}$ correspond to the resonant surfaces $q(r) = m/n$. When the corresponding perturbation is included, the contours of the total helical flux are used to identify the O points, X points and separatrix structures of magnetic islands (Yu 1997).

Given the initial profiles, the three-dimensional initial-value code MHD@Dalian is utilised to solve equations in this work. For the spatial discretisation, the finite

Downloaded from https://www.cambridge.org/core. UNIVERSIDAD AUTONOMA METROPOLITANA, on 19 Nov 2026 at 14:11:34, subject to the Cambridge Core terms of use, available at https://www.cambridge.org/core/terms. https://doi.org/10.1017/S0022377826102025

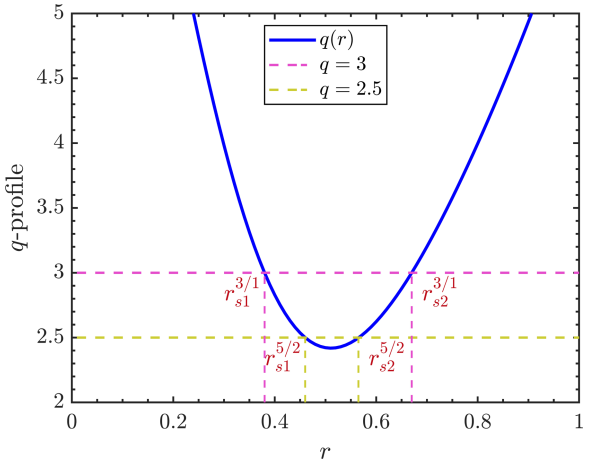


FIGURE 1. The safety factor q-profile with $r_{s1}^{3/1}$, $r_{s2}^{3/1}$ and $r_{s1}^{5/2}$, $r_{s2}^{5/2}$ indicating the inner and outer rational surfaces of the $m/n = 3/1$ and $m/n = 5/2$ modes, respectively.

difference method is adopted in the radial direction, and the pseudospectral method is employed in the poloidal and axial directions; the time advancement employs a two-step predictor–corrector method. An ideally conducting wall condition is assumed at the radial boundary, i.e. satisfying $\tilde{\psi}_{m,n} = \tilde{\phi}_{m,n} = \tilde{u}_{m,n} = \tilde{p}_{m,n} = 0$ at $r = 1$. The MH nonlinear simulations are performed in this paper, and the ranges of poloidal and toroidal mode numbers included in the calculations are $0 \le m \le 24$ and $0 \le n \le 8$, respectively. As shown in figure 1, the initial safety factor q profile is set with typical RMS characteristics, where two pairs of rational surfaces with different helicities (corresponding to $h = 3/1$ and $h = 5/2$, respectively) coexist in the radial direction. The computational domain is discretised with $N_r = 1500$ radial grid points. Other fixed parameters are $S_A^{-1} = 5 \times 10^{-6}$, $R^{-1} = 1 \times 10^{-6}$, the inverse aspect ratio $\varepsilon_a = a/R_0 = 0.25$, $\chi_\parallel = 10$ and $\chi_\perp = 10^{-6}$. The present numerical set-up follows the parameter range commonly used in previous reduced MHD simulations of long-time DTM/NDTM evolution in RMS plasmas. Similar values of S_A^{-1}, R^{-1}, $\chi_\parallel$ and $\chi_\perp$ have been adopted in earlier studies of intermittent DTM bursts, and the MHD@Dalian code has been benchmarked and applied to nonlinear NDTM dynamics in RMS configurations. In these previous applications, the cylindrical reduced MHD formulation has provided a useful framework for isolating the essential nonlinear processes of tearing mode evolution, including rational surface reconnection, mode coupling, bootstrap current effects and q-profile recovery. Following this framework, the adopted dissipation and transport coefficients are kept fixed in all SH/MH and f_b-scan cases, so that the relative effects of MH coupling and bootstrap current fraction are compared under the same numerical and dissipative conditions. The radial resolution $N_r = 1500$ and the spectral range $0 \le m \le 24$, $0 \le n \le 8$ are sufficient for resolving the dominant 3/1 mode, the subdominant 5/2 mode and the main coupled harmonics discussed in the following (Wang *et al.* 2022*a*; Ren *et al.* 2024). Although toroidal curvature, Shafranov shift and neoclassical viscosity beyond the bootstrap current contribution are not explicitly retained in this cylindrical formulation, they are expected to play an important role in determining the quantitative behaviour of realistic tokamak plasmas

Downloaded from https://www.cambridge.org/core. UNIVERSIDAD AUTONOMA METROPOLITANA, on 19 Nov 2026 at 14:11:34, subject to the Cambridge Core terms of use, available at https://www.cambridge.org/core/terms. https://doi.org/10.1017/S0022377826102025

(Hahm 1988; Nishimura, Callen & Hegna 1998; Lütjens *et al.* 2001). These effects may modify the linear growth rates, nonlinear saturation levels and transition values, while the qualitative nonlinear trends discussed in the following are governed primarily by magnetic topology, modal energy redistribution and current profile evolution. Direct quantitative comparisons with JET, EAST and HL-2A experiments or toroidal simulations are beyond the current scope. However, this framework is fully sufficient for isolating the underlying nonlinear mechanisms. Benchmarking against experimental data and cross-code verification will be systematically pursued as the primary focus of future research.

3. Numerical results

In this section, the intermittent bursts and nonlinear coupling phenomena of NDTMs in the RMS configuration are systematically investigated via both MH and SH simulations based on the safety factor profile introduced in § 2.

The SH simulation is first performed with an $m/n = 3/1$ mode initial perturbation, neglecting the bootstrap current ($f_b = 0$). The time evolutions of the kinetic and magnetic energy of the 3/1 mode and its higher harmonics, as well as the safety factor profile, are shown in figure 2(*a–c*). After the first explosive burst at $t = 0.3 \times 10^4$, the system enters the nonlinear phase. The intermittent burst period starting at $t = 0.5 \times 10^4$ is selected as the first intermittent burst for analysis. During each burst, the kinetic and magnetic energy increase rapidly and then decay after reaching their peak values. Meanwhile, the safety factor between the two 3/1 rational surfaces is lifted to greater than 3, causing the resonant surfaces to disappear temporarily. As the ohmic current recovers, the q profile gradually returns to the initial unstable state, and the next intermittent burst is then triggered.

Figure 3 displays the helical magnetic flux contours, the velocity vector field and the stream function contours for the SH simulation with $f_b = 0$. At $t = 0.52 \times 10^4$, magnetic islands are formed on the two rational surfaces. At $t = 0.54 \times 10^4$, the magnetic islands grow continuously; the outer magnetic islands move inward while the inner ones move outward. Consequently, the open magnetic field lines between the inner and outer islands reconnect. The plasma velocity is directed from the X points towards the O points, and the velocity field reaches its maximum at the X points of the magnetic islands where the stream function contours are most concentrated. At $t = 0.55 \times 10^4$, the radial positions of the inner and outer islands are exchanged, and a magnetic separatrix reappears between the islands. Finally, at $t = 0.56 \times 10^4$, the magnetic islands are almost completely consumed, and the open magnetic field lines reappear, indicating that the intermittent burst is approaching its end.

In the MH simulation without bootstrap current ($f_b = 0$), initial perturbations of both the 3/1 and 5/2 modes are introduced. The coexistence of different helicities alters the nonlinear evolution of the system. The time evolutions of the kinetic and magnetic energies of the 3/1 mode, the 5/2 mode and the high-order harmonics, together with the safety factor profile, are shown in figure 4(*a–c*). To further illustrate the redistribution of perturbation energy among different helicities, figure 5 presents the kinetic energy partition ratios, where the total kinetic energy is divided into three parts: the 3/1 mode and its higher harmonics; the 5/2 mode and its higher harmonics; and the coupled modes generated by nonlinear interaction. In the early phase of the evolution, since the distance between the two rational surfaces of the 5/2 mode is smaller, its linear growth rate is higher than that of the 3/1 mode. Consequently, the 5/2 mode reaches saturation first at $t = 0.2 \times 10^4$. This is also reflected in

Downloaded from https://www.cambridge.org/core. UNIVERSIDAD AUTONOMA METROPOLITANA, on 19 Nov 2026 at 14:11:34, subject to the Cambridge Core terms of use, available at https://www.cambridge.org/core/terms. https://doi.org/10.1017/S0022377826102025

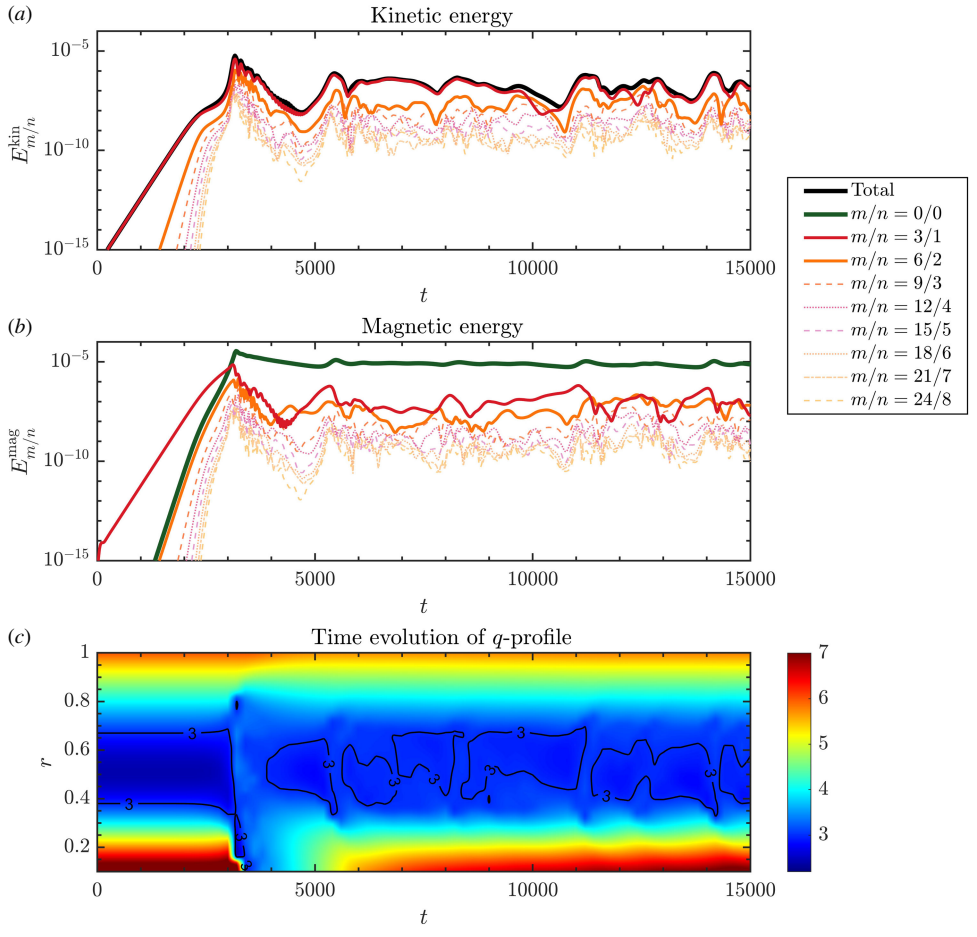


FIGURE 2. (*a*) Time evolutions of kinetic energy $E^{kin}_{m/n}$ and (*b*) time evolutions of the magnetic energy $E^{mag}_{m/n}$ for different harmonics and (*c*) dynamic change of the safety factor profile in the SH simulation for $f_b = 0$.

figure 5, where the 5/2 mode and its higher harmonics occupy the dominant part of the non-axisymmetric kinetic energy during the early nonlinear stage. At this time, the 3/1 mode is still growing. When the 5/2 mode saturates, the growth rate of the 3/1 mode exhibits a transient increase, which is associated with nonlinear coupling induced by the saturated 5/2 mode. As the system approaches the first burst, the energy fraction of the 3/1 mode and its higher harmonics rises rapidly, while the coupled modes also show a finite transient contribution. This indicates that, in the MH case, the perturbation energy is not confined to a single 3/1 harmonic chain, but is distributed through additional nonlinear energy channels associated with the 5/2 mode and the coupled modes. After this transient coupling stage, the 3/1 mode enters the Rutherford regime and subsequently undergoes the first explosive burst. Meanwhile, the modes generated by the coupling between the 5/2 and 3/1 modes, such as the 8/3 mode, also reach saturation. As shown in figure 4(*c*), the burst of the 3/1 mode causes the q profile between the resonant surfaces to rise rapidly and become flattened to greater than $q = 3$. This modification causes the

Downloaded from https://www.cambridge.org/core. UNIVERSIDAD AUTONOMA METROPOLITANA, on 19 Nov 2026 at 14:11:34, subject to the Cambridge Core terms of use, available at https://www.cambridge.org/core/terms. https://doi.org/10.1017/S0022377826102025

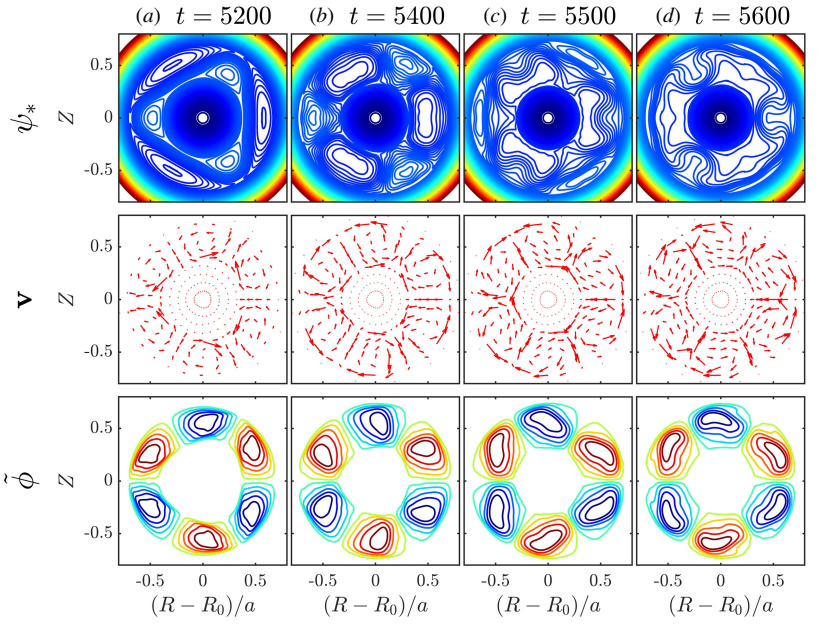


FIGURE 3. Typical helical magnetic flux contours, ψ_* (i); velocity vector fields $\boldsymbol{v}$ (ii); and stream function contours, $\tilde{\phi}$ (iii) at different time slices during the intermittent bursts in the SH simulation for $f_b = 0$.

resonant surfaces satisfying $q = 2.5$ to disappear within the plasma region. Therefore, although residual perturbation energy remains in the system, the 5/2 mode cannot be sustained without its resonance condition, and its amplitude gradually decreases until it is suppressed. The system finally returns to an intermittent bursting phase dominated by the 3/1 mode and its higher harmonics, exhibiting an evolution behaviour similar to that in the SH case.

Figure 6 presents the Poincaré plots, velocity vector fields and stream function contours for the MH simulation with $f_b = 0$. After entering the nonlinear phase, since the distance between the rational surfaces of the 5/2 mode is small, it grows faster than the 3/1 mode. At $t = 1500$, the 5/2 mode has saturated and exhibits an exchange of inner and outer islands, accompanied by an oscillation in kinetic and magnetic energy. At $t = 2100$, as the 3/1 mode continues to grow and its magnetic islands become sufficiently large, perturbations from both modes can be observed in the stream function and velocity vector fields. Simultaneously, the spatial overlap of the 3/1 and 5/2 modes, as well as the high-order magnetic islands (e.g. 8/3 mode) generated by their coupling, induces strong magnetic stochasticity between the resonant surfaces of the 3/1 and 5/2 modes. At $t = 2800$, the 3/1 mode grows to saturation and undergoes the first explosive burst. The energy of the modes generated by the coupling of the 3/1 and 5/2 modes also reach its maximum, and the range influenced by magnetic stochasticity becomes maximal. At $t = 5000$, due to the suppression of other modes by the 3/1 mode, only the intermittent oscillation dominated by the 3/1 mode exists, as evidenced by the Poincaré plots, the velocity vector fields and the stream function contours where only the magnetic islands and perturbations of the 3/1 mode remain while the magnetic stochasticity and magnetic islands of other modes have disappeared.

Downloaded from https://www.cambridge.org/core. UNIVERSIDAD AUTONOMA METROPOLITANA, on 19 Nov 2026 at 14:11:34, subject to the Cambridge Core terms of use, available at https://www.cambridge.org/core/terms. https://doi.org/10.1017/S0022377826102025

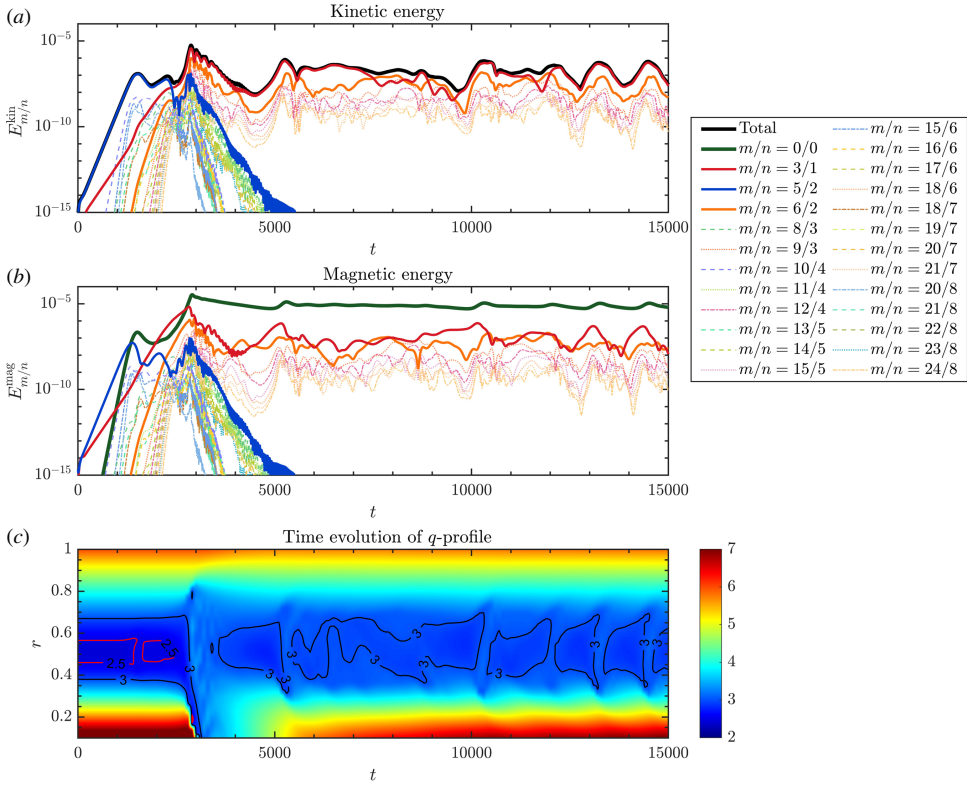


FIGURE 4. (*a*) Time evolutions of kinetic energy $E^{kin}_{m/n}$ and (*b*) time evolutions of the magnetic energy $E^{mag}_{m/n}$ for different harmonics and (*c*) dynamic change of the safety factor profile in the MH simulation for $f_b = 0$.

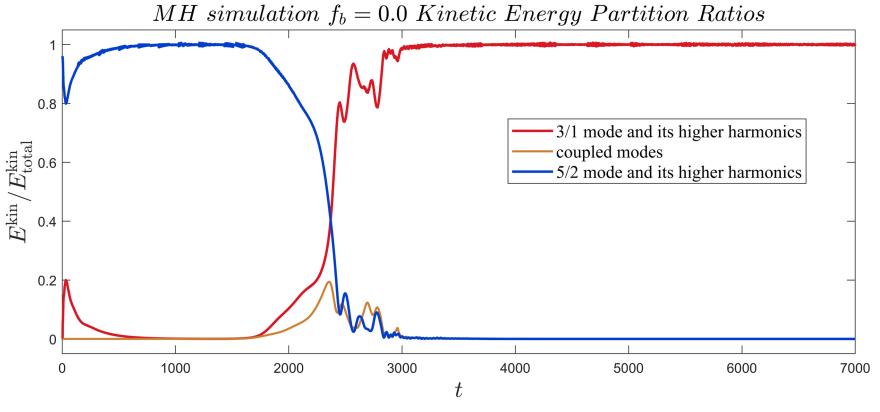


FIGURE 5. Kinetic energy partition ratios in the MH simulation with $f_b = 0$. The total kinetic energy is divided into three parts: the $3/1$ mode and its higher harmonics; the $5/2$ mode and its higher harmonics; the coupled modes generated by nonlinear interaction.

Downloaded from https://www.cambridge.org/core. UNIVERSIDAD AUTONOMA METROPOLITANA, on 19 Nov 2026 at 14:11:34, subject to the Cambridge Core terms of use , available at https://www.cambridge.org/core/terms. https://doi.org/10.1017/S0022377826102025

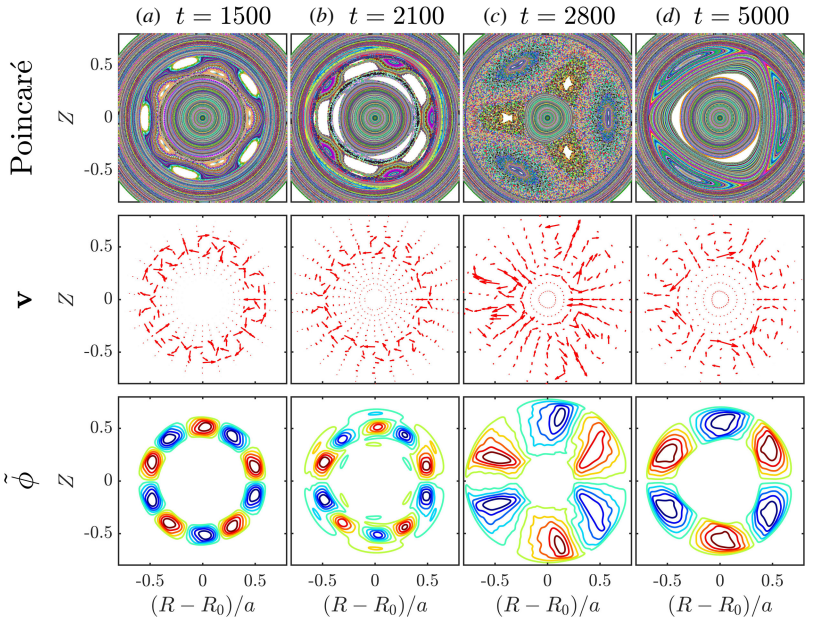


FIGURE 6. Poincaré plots of magnetic field lines in a poloidal cross-section (i); velocity vector fields, $\boldsymbol{v}$ (ii), and stream function contours, $\tilde{\phi}$ (iii) at different time slices in the MH simulation for $f_b = 0$.

With increasing f_b, the results of kinetic energy, magnetic energy and safety factor profiles for SH and MH simulations with $f_b = 0.2$ are shown in figures 7(*a–c*) and 8(*a–c*), respectively. During the intermittent oscillation process after the first explosive burst, it is observed that the amplitudes of kinetic and magnetic energy and the distance between the inner and outer resonant surfaces are significantly reduced compared with those in the $f_b = 0$ case. This is attributed to the fact that, under the condition of maintaining the total current constant, as f_b increases, the proportion of the ohmic current in the source term E_{z0}, which is responsible for restoring the unstable q-profile, decreases. Therefore, the capability of the system to restore the magnetic configuration is weakened, the distance between rational surfaces cannot fully return to the initial equilibrium position and the intensity of subsequent bursts is reduced.

Furthermore, with increasing f_b, the MH evolution appears to exhibit an additional coupling related acceleration effect. As shown by the kinetic energy evolution in the MH simulation with $f_b = 0.2$ (figure 8*a*), when the 5/2 mode reaches saturation, the growth rate of the 3/1 mode increases and remains at an elevated level, so that the 3/1 mode directly enters the Rutherford regime and undergoes the first explosive burst. This behaviour is distinct from the $f_b = 0$ case (figure 4*a*), where the saturation of the 5/2 mode causes only a momentary increase in the growth rate of the still unsaturated 3/1 mode, after which the growth rate returns to its previous level before the 3/1 mode continues its evolution towards the Rutherford regime. This difference suggests that, in the presence of bootstrap current, nonlinear mode coupling can provide an additional drive for the dominant mode and thereby accelerate its entry into the first burst.

Downloaded from https://www.cambridge.org/core. UNIVERSIDAD AUTONOMA METROPOLITANA, on 19 Nov 2026 at 14:11:34, subject to the Cambridge Core terms of use, available at https://www.cambridge.org/core/terms. https://doi.org/10.1017/S0022377826102025

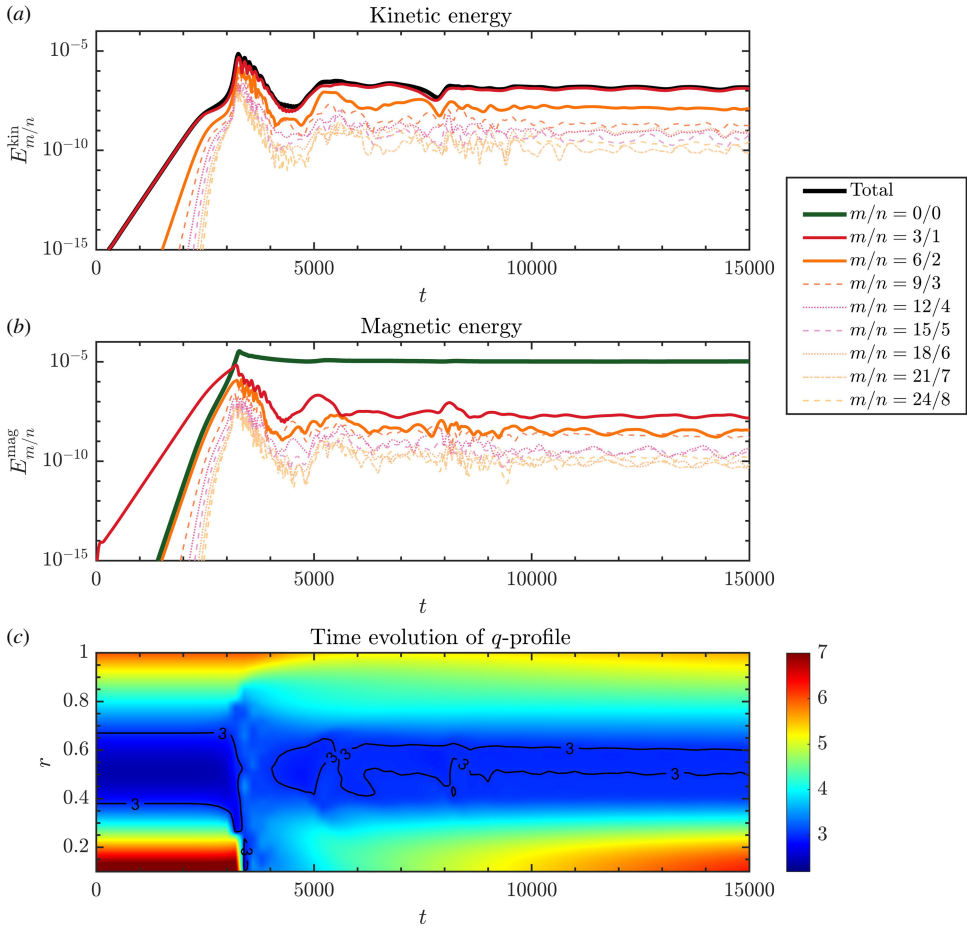


FIGURE 7. (*a*) Time evolutions of kinetic energy $E^{kin}_{m/n}$ and (*b*) time evolutions of the magnetic energy $E^{mag}_{m/n}$ for different harmonics and (*c*) dynamic change of the safety factor profile in the SH simulation for $f_b = 0.2$.

When the bootstrap current fraction is further increased to $f_b = 0.4$, the intermittent bursting phenomenon disappears, as shown in the SH simulation (figure 9*a–c*) and the MH simulation (figure 10*a–c*). Due to the reduced ohmic current contribution in the source term, the flattening of the q profile induced by reconnection cannot be effectively reversed. Simulation results indicate that after the first explosive burst, the safety factor is gradually raised to greater than 3, and the unstable condition for the DTM is no longer satisfied. The kinetic and magnetic energy of the 3/1 mode, 5/2 mode and high-order harmonics exhibit a monotonic decreasing trend, and the system tends towards a stable state.

Figure 11(*a–c*) presents a comparison of the average energy, average amplitude and average period of the intermittent bursts between the SH and MH simulations. From figures 11(*a*) and 11(*b*), it can be seen that the average energy and burst amplitude of the dominant mode (3/1 mode) in the MH simulation are lower than those in the SH simulation. This can be attributed to the redistribution of perturbation energy in the MH case. Starting from the same initial state, part of the energy is

Downloaded from https://www.cambridge.org/core. UNIVERSIDAD AUTONOMA METROPOLITANA, on 19 Nov 2026 at 14:11:34, subject to the Cambridge Core terms of use , available at https://www.cambridge.org/core/terms. https://doi.org/10.1017/S0022377826102025

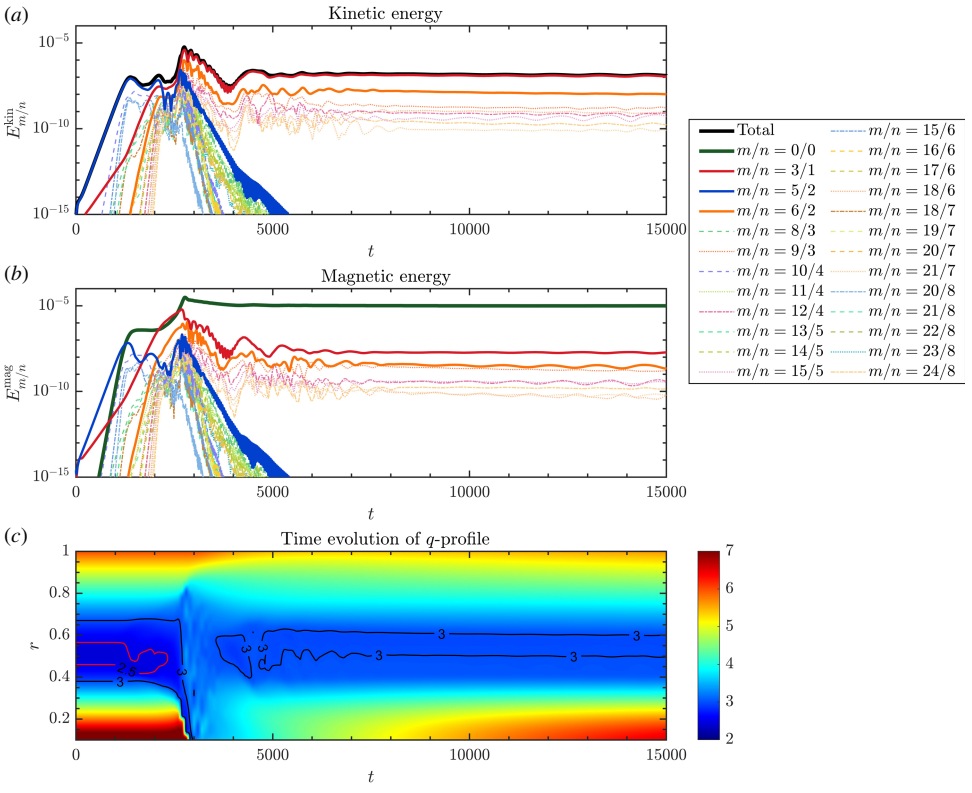


FIGURE 8. (*a*) Time evolutions of kinetic energy $E^{kin}_{m/n}$ and (*b*) time evolutions of the magnetic energy $E^{mag}_{m/n}$ for different harmonics and (*c*) dynamic change of the safety factor profile in the MH simulation for $f_b = 0.2$.

distributed to the 5/2 mode and the higher-order harmonics generated by nonlinear coupling in the early stage of the evolution, thereby reducing the energy available to the dominant 3/1 mode and resulting in lower average burst energy and amplitude than in the SH case.

The bootstrap current fraction has an important impact on the energy intensity of the intermittent bursts. As the bootstrap current fraction increases while the total current is kept constant, the ohmic current contribution to restoring the magnetic configuration decreases, so that the q-profile becomes less capable of returning to its initial unstable state between two bursts. Consequently, the distance between the two rational surfaces decreases, and so does the spatial extent of the corresponding perturbation velocity fields, as shown in figure 12. As a result, the system can accumulate less energy between intermittent bursts, and the energy released during each reconnection event is also reduced, leading to a decreasing trend in the average energy and the average amplitude with increasing f_b. Meanwhile, because the recovery towards the next unstable state becomes slower, the time required to trigger the subsequent burst is prolonged, and thus the burst period increases with the bootstrap current fraction.

Furthermore, in the present equilibrium, when the bootstrap current fraction increases to approximately $f_b = 0.2$, the intermittent bursts of the dominant mode

Downloaded from https://www.cambridge.org/core. UNIVERSIDAD AUTONOMA METROPOLITANA, on 19 Nov 2026 at 14:11:34, subject to the Cambridge Core terms of use , available at https://www.cambridge.org/core/terms. https://doi.org/10.1017/S0022377826102025

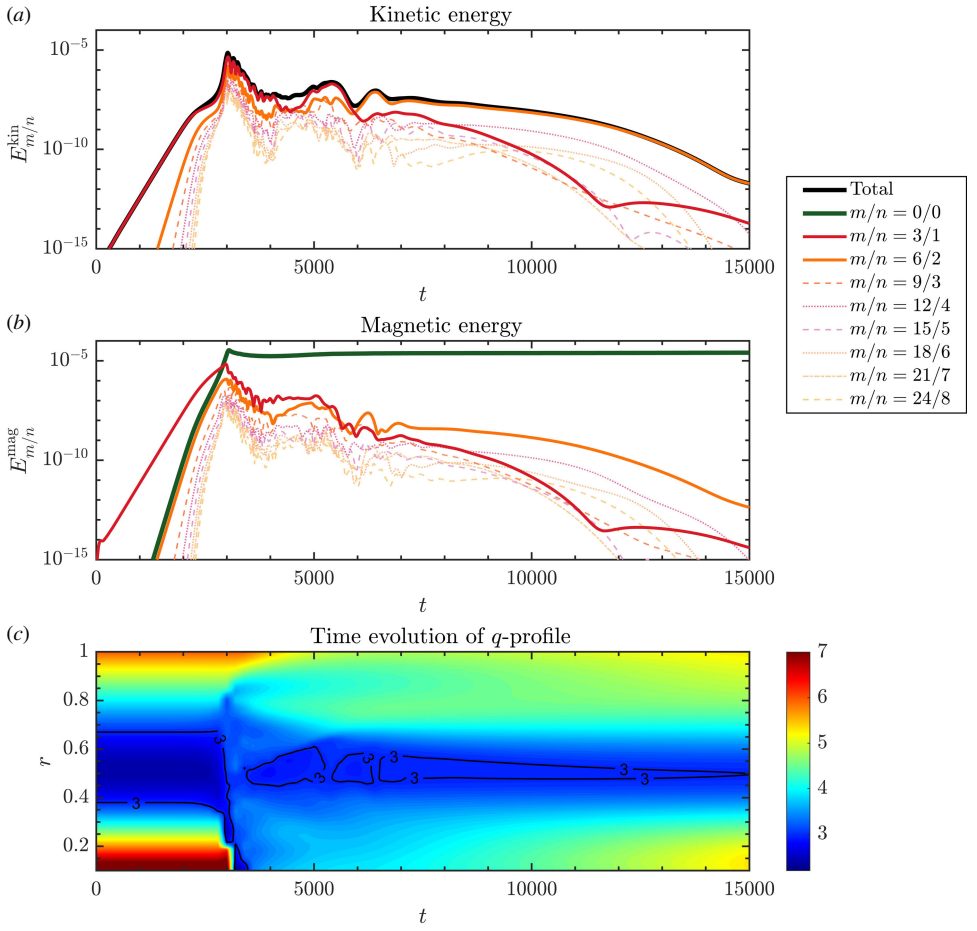


FIGURE 9. (*a*) Time evolutions of kinetic energy $E^{kin}_{m/n}$ and (*b*) time evolutions of the magnetic energy $E^{mag}_{m/n}$ for different harmonics and (*c*) dynamic change of the safety factor profile in the SH simulation for $f_b = 0.4$.

exhibit a different nonlinear pattern: the burst amplitude tends to saturate, while the burst period gradually decreases. This transition is closely related to the competition between reconnection induced q-profile relaxation and ohmic current driven profile restoration. As f_b increases while the total current is kept fixed, the ohmic current contribution in $E_{z0} = S_A^{-1}(j_0 - j_{b0})$ decreases, and the recovery of the q profile becomes increasingly limited. Under this condition, the system still remains in an intermittent bursting state, but the bursts evolve into a smaller amplitude form on a lower energy basis. As a result, the energy accumulated and released in each cycle remains constrained, leading to the saturation of the burst amplitude. Meanwhile, because the excursion of each intermittent burst becomes smaller, the dominant mode can reach the next reconnection condition over a shorter interval, and the burst period therefore decreases gradually.

Further comparison between the SH and MH simulation results reveals that under higher bootstrap current conditions, both the average amplitude and the average period of the dominant mode in the MH system are significantly smaller than those

Downloaded from https://www.cambridge.org/core. UNIVERSIDAD AUTONOMA METROPOLITANA, on 19 Nov 2026 at 14:11:34, subject to the Cambridge Core terms of use , available at https://www.cambridge.org/core/terms. https://doi.org/10.1017/S0022377826102025

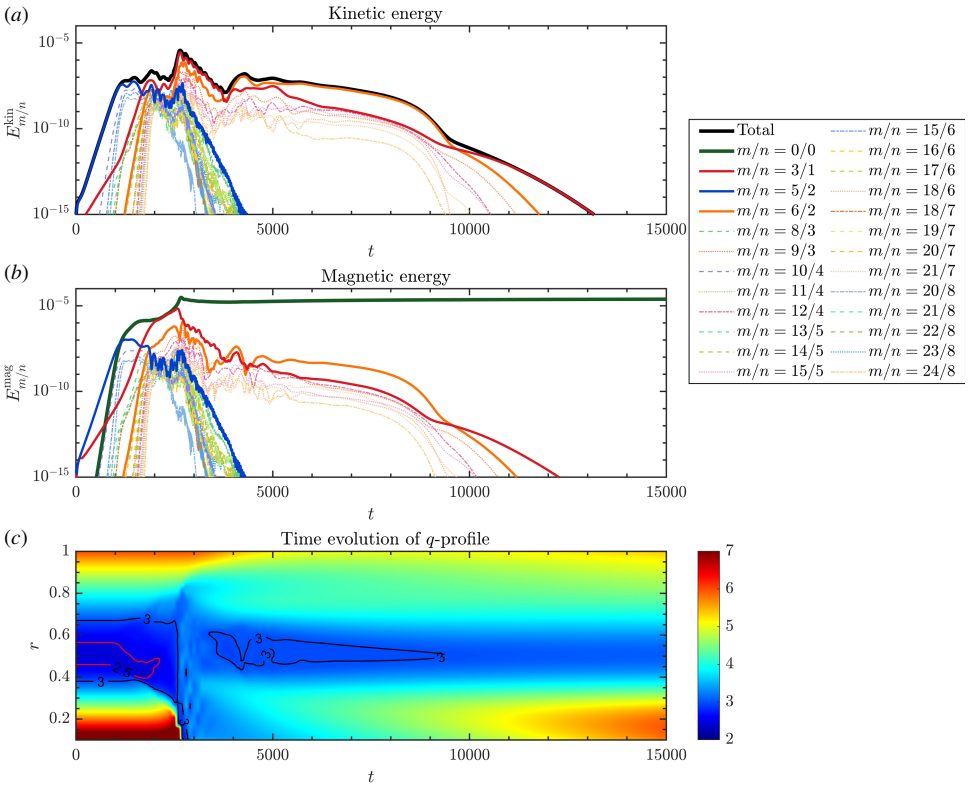


FIGURE 10. (*a*) Time evolutions of kinetic energy $E^{kin}_{m/n}$ and (*b*) time evolutions of the magnetic energy $E^{mag}_{m/n}$ for different harmonics and (*c*) dynamic change of the safety factor profile in the MH simulation for $f_b = 0.4$.

in the SH case. For example, in the present equilibrium, at $f_b = 0.4$, the average amplitude is reduced by approximately 46.18 %, and the burst period is shortened by approximately 30.56 %. At this bootstrap current fraction, the ohmic restoration is further weakened, so that the system can hardly re-establish a strongly unstable double tearing configuration after the first crash. This difference also reflects the evolutionary characteristics of the MH system. In the early phase of the MH evolution, part of the perturbation energy is distributed into the 5/2 mode and its higher harmonics as well as the coupled modes, so that the burst intensity of the dominant mode is lower than that in the SH case. After entering the nonlinear phase, the coupled modes in the MH system are significantly suppressed, and the system eventually evolves into a state dominated by the 3/1 mode and its higher harmonics. Under high bootstrap current conditions, the kinetic and magnetic energies of this dominant mode show a decreasing trend during the subsequent evolution. As a result, the overall energy level of the dominant mode remains relatively low, so that the system exhibits weaker relaxation behaviour and a shorter burst period than in the SH case. Since the balance between q-profile relaxation and restoration is determined by the equilibrium q profile, the pressure gradient driven bootstrap current and the separation between rational surfaces, the transition values observed here are expected to depend on the selected equilibrium configuration.

Downloaded from https://www.cambridge.org/core. UNIVERSIDAD AUTONOMA METROPOLITANA, on 19 Nov 2026 at 14:11:34, subject to the Cambridge Core terms of use , available at https://www.cambridge.org/core/terms. https://doi.org/10.1017/S0022377826102025

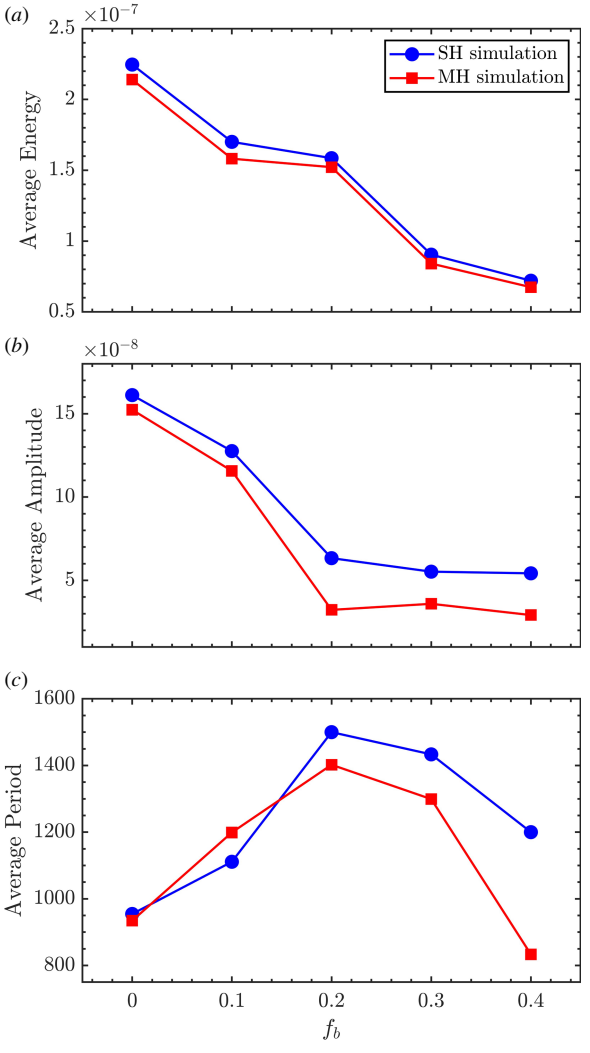


FIGURE 11. Comparisons of (*a*) the average energy, (*b*) the average amplitude and (*c*) the average period of intermittent bursts in the SH and MH simulations with different bootstrap current fractions. The statistical interval is selected from the first energy minimum after the initial explosive burst to the last energy minimum before $t = 15\,000$. Within this interval, the average energy is obtained by time-averaging the dominant mode energy; the average amplitude is calculated as the mean peak to valley energy variation of each burst cycle; and the average period is evaluated from the mean time interval between adjacent energy peaks.

4. Summary

In this work, the nonlinear dynamic evolution of intermittent bursts induced by NDTMs in RMS configurations is systematically investigated using a three-dimensional reduced MHD model in a cylindrical coordinate system. During the long-pulse evolution, the system does not tend to be completely stable after experiencing the initial fast reconnection, but exhibits continuous intermittent bursts. During each burst, the violent change of the magnetic flux topology and the reconnection of magnetic field lines on the rational surfaces are accompanied by a rapid

Downloaded from https://www.cambridge.org/core. UNIVERSIDAD AUTONOMA METROPOLITANA, on 19 Nov 2026 at 14:11:34, subject to the Cambridge Core terms of use, available at https://www.cambridge.org/core/terms. https://doi.org/10.1017/S0022377826102025

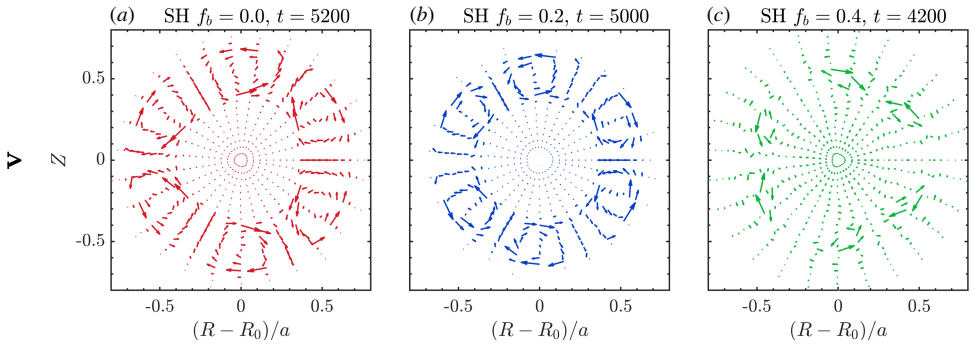


FIGURE 12. Velocity vector fields ($\boldsymbol{v}$) during the intermittent oscillation process in the SH simulation with different bootstrap current fractions: (*a*) $f_b = 0$; (*b*) $f_b = 0.2$; (*c*) $f_b = 0.4$.

increase in the kinetic energy of the system. Meanwhile, the safety factor q profile undergoes a fast local relaxation and is elevated up between the two rational surfaces. After the burst, under the continuous effect of the ohmic current, the q profile slowly recovers to the initial unstable state, thereby periodically triggering the next magnetic island reconnection and energy release.

Comparisons between the SH and MH simulation results reveal that the burst amplitude and average energy of the dominant mode (3/1 mode) in the MH case are significantly lower than those in the SH case. This phenomenon is mainly attributed to the redistribution of perturbation energy during the MH nonlinear coupling process: in the early phase of the system evolution, a portion of the magnetic free energy is transferred to the subdominant mode (such as the 5/2 mode) and the higher harmonics generated by mode coupling, which effectively weakens the available energy of the dominant mode. In addition, the nonlinear mode coupling in the MH case provides an extra drive for the dominant mode, increasing its growth rate and accelerating its entry into the Rutherford regime, thereby bringing forward the first explosive burst.

This work further investigates the influence of the bootstrap current fraction on the evolutionary characteristics of the intermittent bursts. The results indicate that increasing the bootstrap current fraction weakens the ohmic current contribution in the source term responsible for restoring the magnetic configuration, thus reducing the ability of the q profile to recover to the strongly unstable state. This leads to an overall reduction in the average kinetic energy and amplitude of the intermittent bursts. In particular, when the bootstrap current fraction increases to a certain threshold ($f_b \geq 0.2$ in this work), the evolution of the dominant mode exhibits the characteristics that the amplitude tends to saturate and the period decreases gradually. Under this high bootstrap current fraction condition, since the overall energy level of the dominant mode in the MH system is further suppressed, the system can only maintain relatively weak relaxation oscillations. Therefore, it exhibits a smaller burst amplitude and a shorter evolutionary period than the SH case.

These results indicate that, for high bootstrap current plasmas with multiple rational surfaces, long-time MHD stability cannot be fully evaluated within an SH framework. Instead, the combined influence of MH coupling and neoclassical effects should be considered, especially for advanced tokamak scenarios aiming at long-pulse steady-state operation. The present results also provide a process-focused reference for understanding how different helicities participate in the nonlinear

Downloaded from https://www.cambridge.org/core. UNIVERSIDAD AUTONOMA METROPOLITANA, on 19 Nov 2026 at 14:11:34, subject to the Cambridge Core terms of use, available at https://www.cambridge.org/core/terms. https://doi.org/10.1017/S0022377826102025

relaxation process and how the recovery of the q profile affects the recurrence of intermittent bursts. Future toroidal simulations incorporating toroidal curvature, Shafranov shift and neoclassical viscosity, together with realistic equilibrium profiles, will be useful for further testing and extending the present conclusions under more realistic conditions. Although the present study focuses on isolating the underlying physical processes, comparing these nonlinear trends with experimental discharges in major devices like JET, EAST and HL-2A remains a vital objective. Such comparative analyses and experimental validations will be systematically pursued in our future work.

From an operational perspective, the present results also provide guidance for future control-oriented studies. Since the MH evolution involves not only the dominant 3/1 mode but also the 5/2 mode and coupled harmonics, active control strategies should consider the MH structure of the instability rather than focusing only on a single dominant island. In particular, the redistribution of perturbation energy among different helicities suggests that the timing, deposition position and spectral selectivity of external control should be carefully optimised. Therefore, nonlinear simulations including 'electron cyclotron current drive' and 'resonant magnetic perturbations' effects are needed to assess deposition strategy, phase control and possible control windows for mitigating NDTM induced intermittent bursts in high bootstrap current RMS plasmas in future advanced tokamaks (Tang *et al.* 2020; Liu *et al.* 2024).

Acknowledgements

Editor Tünde Fülöp thanks the referees for their advice in evaluating this article.

Funding

This research is supported by National Key R&D Program of China (grant no. 2024YFE03000102), the National Natural Science Foundation of China (grant nos.12435014 and 12575228) and the Fundament Research Funds for the Central Universities (grant no. DUT25LAB108).

Declaration of interests

The authors report no conflict of interest.

REFERENCES

BARDOCZI, L., DUDKOVSKAIA, A., LA HAYE, R.J., CALLEN, J.D., CHRYSTAL, C. & PODESTA, M. 2024 *Phys. Rev. Lett.* **132**, 065107.

BARDOCZI, L., LOGAN, N.C. & STRAIT, E.J. 2021 *Phys. Rev. Lett.* **127**, 055002.

BIERWAGE, A., HAMAGUCHI, S., WAKATANI, M., BENKADDA, S. & LEONCINI, X. 2005 *Phys. Rev. Lett.* **94**, 065001.

BUTTERY, R.J. *et al.* 2000 *Plasma Phys. Control. Fusion* **42**, B61.

CHANG, Z. *et al.* 1996 *Phys. Rev. Lett.* **77**, 3553.

DONG, J.Q., MAHAJAN, S.M. & HORTON, W. 2003 *Phys. Plasmas* **10**, 3151.

FENG, Y.C., WANG, X.Q., XU, Y., LIU, H.F., HUANG, J., ZHANG, X., LIU, H., CHENG, J. & TANG, C.J. 2020 *Phys. Plasmas* **27**, 114501.

FITZPATRICK, R. 1995 *Phys. Plasmas* **2**, 825.

FUJITA, T. *et al.* 2001 *Phys. Rev. Lett.* **87**, 085001.

FURTH, H.P., RUTHERFORD, P.H. & SELBERG, H. 1973 *Phys. Fluids* **16**, 1054.

GORMEZANO, C. *et al.* 2007 *Nucl. Fusion* **47**, S285.

Downloaded from https://www.cambridge.org/core. UNIVERSIDAD AUTONOMA METROPOLITANA, on 19 Nov 2026 at 14:11:34, subject to the Cambridge Core terms of use, available at https://www.cambridge.org/core/terms. https://doi.org/10.1017/S0022377826102025

HAHM, T.S. 1988 *Phys. Fluids* **31**, 3709.
HAZELTINE, R.D., KOTSCHENREUTHER, M. & MORRISON, P.J. 1985 *Phys. Fluids* **28**, 2466.
HU, Q.M. *et al.* 2023 *Phys. Plasmas* **30**, 020701.
ISHIDA, S., KOIDE, Y., OZEKI, T., KIKUCHI, M., TSUJI, S., SHIRAI, H., NAITO, O. & AZUMI, M. 1992 *Phys. Rev. Lett.* **68**, 1531.
ISHII, Y., AZUMI, M. & KISHIMOTO, Y. 2002 *Phys. Rev. Lett.* **89**, 205002.
JANVIER, M., KISHIMOTO, Y. & LI, J.Q. 2011 *Phys. Rev. Lett.* **107**, 195001.
JARDIN, S.C., FERRARO, N. & KREBS, I. 2015 *Phys. Rev. Lett.* **115**, 215001.
KIKUCHI, M. & AZUMI, M. 2012 *Rev. Mod. Phys.* **84**, 1807.
KUIROUKIDIS, A. & THROUMOULOPOULOS, G.N. 2015 *J. Plasma Phys.* **81**, 905810404.
LEVINTON, F.M. *et al.* 1995 *Phys. Rev. Lett.* **75**, 4417.
LIU, T., WANG, Z.X., WEI, L., WANG, J.L. & REIMAN, A. 2024 *Nucl. Fusion* **64**, 036001.
LÜTJENS, H., LUCIANI, J.-F. & GARBET, X. 2001 *Phys. Plasmas* **8**, 4267.
MATSUMOTO, T., NAITOU, H., TOKUDA, S. & KISHIMOTO, Y. 2005 *Nucl. Fusion* **45**, 1264.
NISHIMURA, Y., CALLEN, J.D. & HEGNA, C.C. 1998 *Phys. Plasmas* **5**, 4292.
PRITCHETT, P.L., LEE, Y.C. & DRAKE, J.F. 1980 *Phys. Fluids* **23**, 1368.
REN, G.Z., WEI, L., LI, J.Q. & WANG, Z.X. 2024 *Nucl. Fusion* **64**, 056016.
SATO, M. & WAKATANI, M. 2005 *Nucl. Fusion* **45**, 143.
STRAIT, E.J. *et al.* 1995 *Phys. Rev. Lett.* **75**, 4421.
STRAUSS, H.R. 1976 *Phys. Fluids* **19**, 134.
TANG, W.K., WANG, Z.X., WEI, L., WANG, J.L. & LU, S.S. 2020 *Nucl. Fusion* **60**, 026015.
VON GOELER, S., STODIEK, W. & SAUTHOFF, N. 1974 *Phys. Rev. Lett.* **33**, 1201.
WANG, H.H., WANG, Z.X., DING, Y.H. & RAO, B. 2015*a* *Plasma Science and Technology* **17**, 539.
WANG, Z.X., WEI, L. & YU, F. 2015*b* *Nucl. Fusion* **55**, 043005.
WANG, H.H., WANG, Z.X. & WANG, X.G. 2013 *J. Plasma Phys.* **80**, 417.
WANG, X.Q. & WANG, X.G. 2015 *Phys. Plasmas* **22**, 102504.
WANG, X.Q., WANG, X.G., XU, W.B. & WANG, Z.X. 2011 *Phys. Plasmas* **18**, 012102.
WANG, Z.X., LIU, T. & WEI, L. 2022*a* *Rev. Modern Plasma Phys.* **6**, 14.
WANG, Z.X., TANG, W.K. & WEI, L. 2022*b* *Plasma Sci. Technol.* **24**, 033001.
WANG, Z.X., WANG, X.G., DONG, J.Q., LEI, Y.A., LONG, Y.X., MOU, Z.Z. & QU, W.X. 2007 *Phys. Rev. Lett.* **99**, 185004.
WEI, L. & WANG, Z.X. 2014*a* *Phys. Plasmas* **21**, 062505.
WEI, L. & WANG, Z.X. 2014*b* *Nucl. Fusion* **54**, 043015.
WEI, L., YANG, X.F., ZHENG, S. & LIU, Y. 2012 *J. Plasma Phys.* **78**, 663.
YU, Q. 1997 *Phys. Plasmas* **4**, 1047.
YU, Q. 2007 *Nucl. Fusion* **47**, 1244.
YU, Q., GÜNTER, S., LACKNER, K., GUDE, A. & MARASCHEK, M. 2000 *Nucl. Fusion* **40**, 2031.
ZARNSTORFF, M.C. *et al.* 1988 *Phys. Rev. Lett.* **60**, 1306.
ZHANG, C.L. & MA, Z.W. 2009 *Phys. Plasmas* **16**, 122113.
ZHANG, W., LIN, X., MA, Z.W., LU, X.Q. & ZHANG, H.W. 2020 *Phys. Plasmas* **27**, 122509.
ZHANG, W., MA, Z.W., ZHU, J. & ZHANG, H.W. 2019 *Plasma Phys. Control. Fusion* **61**, 075002.

Downloaded from https://www.cambridge.org/core. UNIVERSIDAD AUTONOMA METROPOLITANA, on 19 Nov 2026 at 14:11:34, subject to the Cambridge Core terms of use, available at https://www.cambridge.org/core/terms. https://doi.org/10.1017/S0022377826102025